1. TITLE

GIMMS Normalized Difference Vegetation Index

1.1 Data Set Identification

NASA Global Inventory Modeling and Mapping Studies Satellite Drift Corrected and NOAA-16 Incorporated Normalized Difference Vegetation Index (NDVI), Monthly 1981 – 2002.

1.2 Database and Database Table Name(s)

1.3 File Name(s)

gimms_ndvi_xx_YYYMM00.asc
where xx = qd (quarter degree), hd (half degree) and 1d (one degree)

1.4 Revision Date of this Document

November 19, 2003

2. INVESTIGATOR(S)

2.1 Investigator's Name and Title

Compton J. Tucker
NASA-Goddard Space Flight Center
Code 923
Greenbelt, MD 20771

Jorge E. Pinzon
Science Systems and Applications
NASA-Goddard Space Flight Center
Code 923
Greenbelt, MD 20771

Molly E. Brown
Science Systems and Applications
NASA-Goddard Space Flight Center
Code 923
Greenbelt, MD 20771

2.2 Title of Investigation

Monitoring Seasonal and interannual variations in Land-Surface Vegetation from 1981-2002 using GIMMS NDVI .

2.3 Contacts

	Contact 1	Contact2
2.3.1 Name	Dr. Compton Tucker	Jorge E. Pinzon
2.3.2 Address	NASA-Goddard Space Flight Center	NASA-Goddard Space Flight Center
	Code 923	Code 923
City/St.	Greenbelt, MD	Greenbelt, MD
Zip Code	22181	22181
Country	USA	USA
2.3.3 Tel. No.	301-614-6644	301-614-6680
Fax No.	301-614-6699	301-614-6699
2.3.4 E-mail	compton@kratmos.gsfc.nasa.gov	pinzon@negev.gsfc.nasa.gov

2.4 Requested Form of Acknowledgment

Please cite the following publications whenever these data are used:

1. Pinion, J., M. E. Brown and C. J. Tucker (2003). "Nonparametric Satellite Drift Correction of NDVI Time Series from NOAA-AVHRR Radiometers Using the Empirical Mode Decomposition." IEEE Transactions Geoscience and Remote Sensing **submitted**.

2. Pinzon paper on NOAA-16 integration…
3. Tucker, C. J., M. E. Brown, R. Mahoney, S. O. Los, N. El Saleous and E. Vermote (2003). "The Global Inventory Mapping and Monitoring 1981-2003 AVHRR 8-Km Dataset." Photogrammetric Engineering and Remote Sensing **in revision**

3.0 Introduction

3.1 Objective/Purpose

The Global Inventory Modelling and Mapping Studies (GIMMS) normalized difference vegetation index (NDVI) data sets were generated to provide a 22-year satellite record of monthly changes in terrestrial vegetation. Using (nonlinear) Empirical Mode Decomposition methods, we reduced NDVI variations arising from atmospheric, calibration, view geometry and other effects not related to actual vegetation change. Global NDVI was generated to provide inputs for computing the time series of biophysical parameters contained in the Initiative II collection. NDVI is used in climate models and biogeochemical models to calculate photosynthesis, the exchange of CO_2 between the atmosphere and the land surface, land-surface evapotranspiration and the absorption and release of energy by the land surface.

3.2 Summary of Parameters

Global, composited, monthly, normalized difference vegetation index over land areas. NDVI is the difference (in reflectance) between the AVHRR near-infrared and visible bands divided by the sum of these two bands (Sellers et al. 1994; Sellers 1985; Tucker 1980).

3.3 Discussion

Because NDVI is a ratio of differences between two adjacent bands, it is largely *insensitive* to variations in illumination intensity. However, NDVI ***is sensitive*** to effects that differ between bands. Band calibrations, for example, have changed frequently between the five NOAA AVHRR instruments that acquired the NDVI record for the 22-year Initiative II period. In addition, natural variability in atmospheric aerosols and column water vapor have affected the NDVI record. Over the period of record there were two major volcanic eruptions, El Chichon in 1982 and Mt. Pinatubo in 1991, that injected large quantities of aerosols into the Earth's stratosphere. These aerosols, along with smoke from biomass burning and dust from soil erosion and other factors, can introduce significant variability in the AVHRR NDVI record. These constituents have significantly different effects on AVHRR band's 1 and 2. The GIMMS NDVI corrects for the known changes of the atmosphere from these two volcanic eruptions, but reductions in the NDVI

signal can still be seen over densely vegetated tropical land covers for limited time periods.

NDVI is also sensitive to the periodic variations in solar illumination angle and sensor view angles induced by the NOAA orbits. Its polar, sun-synchronous orbits permitted daily coverage of each point on earth, although at time-varying viewing and illumination geometry. The GIMMS NDVI dataset has a satellite overpass time drift correction that largely eliminates the variation of NDVI due to changes in solar zenith angle.

Frequent cloud cover can also create numerous gaps in the daily AVHRR record eliminating roughly 2/3s of the data. In order to construct cloud-free views of the Earth, **composite** images were constructed at regular intervals by selecting pixels with the maximum NDVI during regularly spaced intervals. Choosing pixels with maximum NDVI reduces cloud cover and water vapor effects since both strongly reduce NDVI. Compositing can be done over any time interval, but 9-10 days is generally selected as the minimum period since the NOAA orbit repeats at that frequency. The GIMMS data record constructed here is based on 15 day composites. There are two 15 day composites per month, the first for day 1-15, and the second for day 16 to the end of the month. We have taken the mean of the two fifteen day composites to represent the month.

4. THEORY OF ALGORITHM/MEASUREMENTS

Green leaves have a higher reflectance in the AVHRR near infrared band (band 2) than in the visible band (band 1), because of differences in leaf chlorophyll absorption between the two bands. Chlorophyll absorbs strongly in the red region, spanned by AVHRR band 1. Thus, the difference in vegetation reflectance between the near infrared and visible bands increases with green leaf vegetation density, hence chlorophyll concentration. The ratio of the difference between band 2 and band 1 and their sum, hence the NDVI, is an index that ranges between -1 and +1; the observed range is usually smaller: Non-vegetated materials generally have a much lower NDVI (around 0) than dense vegetation (>0.7), since their near infrared and visible reflectances are more nearly equal.

5. EQUIPMENT

5.1 Instrument Description.

The Advanced Very High Resolution Radiometer (AVHRR) acquired data in 5 spectral bands; one visible, one near infrared and three thermal bands, all with 1024 quantizing levels. The thermal bands are not used in the GIMMS NDVI data. The AVHRR produces at 1.1 and 4 km spatial resolution. The 4 km product or global area coverage (GAC) product is derived from the 1 km product by onboard sampling. The 4 km product is available globally from July 1981 until the present. The 1 km record is not continuous. Its availability depends upon prior arrangements made by NOAA, or on the proximity of a local receiving station that can capture the data directly from the satellite.

5.1.1 Platform

The NOAA AVHRR satellite series 7,9, 11, 14 and 16 used for the Initiative II NDVI record flew in sun-synchronous polar orbits with a nominal 1:30 or 2:30 pm local daytime overpass time at launch. However, the overpass times drifted by 1-2 minutes per month to as much as 4 1/2 hours later in the day creating variable illumination and view angles over the period of record. The 55-degree sensor swath width permitted a daily view of each pixel on Earth although at different illumination and view angles during the 9-day repeat cycle. Maximum value NDVI data compositing tends to select pixels acquired in a near-nadir mode with minimum atmospheric effects. Even so, view, illumination and atmospheric effects remain. Reducing these effects was the aim of GIMMS processing.

5.1.2 Mission Objectives

The NOAA AVHRR satellite sensor series was originally designed as a weather satellite. However from the early 1980s, AVHRR data has found increasing use to monitor the type and condition of land vegetation. AVHRR vegetation data archives extend back to August 1981.

5.1.3 Key Variables

The AVHRR measured top of the atmosphere radiance in 5 bands. Band 1 covered the 0.5 to 0.7 um region, band 2 the 0.7 to 1.1 um region, with three thermal bands one covering the middle infrared region around 3 microns and two thermal infrared bands in the 10 to 11 micron region. The GIMMS NDVI product uses as input radiance in bands 1 and 2 and were mapped at the NASA Goddard Space Flight Center under the guidance of Dr. Compton Tucker. The current adjusted NDVI dataset was derived entirely from the NDVI produced during the 1998-2000 remapping effort of the GIMMS group.

5.1.4 Principles of Operation

The NOAA satellite series, NOAA 6, 7, 9, 11 and 14 were in polar, sun-synchronous orbits with nadir afternoon overpass times. NOAA 7 data span the years 1981 -1985, NOAA 9, 1986-1989, NOAA 11, 1989-1995, NOAA 14, 1995-2000, and NOAA-16 from 2000 to 2004 (and continues through the present). Data from NOAA-9 was used from September 1994 until January 1995 when NOAA 11 started to malfunction and its replacement, NOAA 13, failed shortly after launch. Each AVHRR sensor has different and variable calibration and overpass time.

5.1.5 Instrument Measurement Geometry

The AVHRR is a scanning, imaging radiometer, scanning ± 55 degrees, providing a 2800 km swath width. The orbital configuration permits daily coverage at a maximum spatial resolution of 1 km of each point on earth, although at different viewing and illumination geometries on subsequent days. The orbit repeats its ground track each 9 days.

5.1.6 Manufacturer of Instrument

See NOAA –KLM users guide for specifications of the newest NOAA AVHRR instrument.
http://www2.ncdc.noaa.gov/docs/klm/

5.2 Calibration.

NOAA provides preflight calibration coefficients that relate the digital counts measured by the satellite to reflectances. The preflight calibration coefficients for the visible and near infrared channel are of the form

reflectance = gain*(digital counts - offset)

The gain and the offset are determined on the ground prior to launch of the satellite; The gain and offset are referred to as preflight calibration coefficients. The preflight calibration coefficients change for each satellite. In some cases preflight coefficients were updated during the time of operation of a satellite.

Preflight calibration coefficients do not take into account the degradation of the AVHRR during its time of operation. Several techniques exist to correct for the change in sensitivity of the AVHRR. For the GIMMS data, the coefficients by Vermote and Kaufman (1995) are used to correct the visible and near infrared reflectances for in-flight sensor degradation. In the GIMMS NDVI data the relative degradation error in the gain is further reduced to below 1 % by using a desert calibration of the ratio of channels 1 and 2 reflectances to invariant Sahara Desert targets.

76. PROCEDURE

6.1 Data Acquisition Methods

The input data for the GIMMS Land data processing is the NOAA AVHRR GAC 1B data. Our GAC 1B data were obtained from NOAA and from NCAR sources at the time of acquision from 1985 to the present. We have augmented this dataset with GAC 1B data available from NOAA's Satellite Active Archive. The GIMMS NDVI datasets were corrected using solar zenith angle values from the AVHRR sensor for the period of 1981-2002 (Pinzon et al. 2003; Tucker et al. 2003).

6.2 Spatial Characteristics.

6.2.1 Spatial Coverage.

The coverage is global. Data in files are ordered from North to south and from West to East beginning at 180 degrees West and 90 degrees North. Point (1,1) represents the grid cell centered at

* 89.5 N and 179.5 W for the 1 by 1 degree data (see section 8.4)

* 89.75 N and 179.75 W for the 0.5 by 0.5 degree (30 minutes by 30 minutes) data (see section 8.4)

* 89.875 N and 179.875 W for the 0.25 by 0.25 degree (15 minutes by 15 minutes) data (see section 8.4)

6.2.2 Spatial Resolution.

The data are given in an equal-angle latitude longitude grid at three different spatial resolutions of 1 x 1, 0.5 x 0.5 and 0.25 x 0.25 degree latitude and longitude.

6.3 Temporal Characteristics.

6.3.1 Temporal Coverage.

The data is available from July 1981 through June 2002.

6.3.2 Temporal Resolution.

Monthly; The GIMMS dataset is composited at a 15-day time step. The monthly data is produced by calculating a mean for each pixel from the corresponding pixel from the two 15-day composites.

7.0 OBSERVATIONS

7.1 Field Notes
Not applicable

8.0 DATA DESCRIPTION

8.1 Table Definition with Comments

8.2 Type of Data

8.2.1 Parameter/ Variable Name	8.2.2 Parameter/ Variable Description	8.2.3 Data Range	8.2.4 Units of Measurement	8.2.5 Data Source
GIMMS NDVI	Normalized Difference	Theoretical range	[Unitless]	AVHRR

	Vegetation Index calculated from AVHRR channel 1 and 2 digital count data.	between -1 and 1; values around 0 for bare soil (low or no vegetation) values of 0.9 or larger for dense vegetation. Water values = -0.1 Bad values = -0.05		

GIMMS Normalized Difference Vegetation Index has been corrected for:

- residual sensor degradation and sensor intercalibration differences;
- distortions caused by persistent cloud cover in tropical evergreen broadleaf forests ;
- solar zenith angle and viewing angle effects;
- volcanic aerosols;
- missing data in the Northern Hemisphere during winter using interpolation;
- short-term atmospheric aerosol effects, atmospheric water vapor effects, and cloud cover.

8.3 Sample Data Record

Not Applicable

8.4 Data Format

8.4.1 NDVI files

NDVI is archived in ASCII format, arranged in columns and rows with a single space between the fields. The 1 degree data has the size 360 x 180, the half degree data files are 720 x 360, and the quarter degree files are 1440 x 720. The projection of the NDVI data files are in Geographic equal angle projection (lat/lon) and their origin is at 180 degrees West, 90 degrees North. There are four significant digits for NDVI, with the values ranging from 0 to 1. Water bodies are coded as –0.1 and missing data over land are coded as –0.05.

8.4.2 DVD NDVI Archive Overview

The DVD file format is ASCII, and consists of numerical fields of varying length, which are space delimited and arranged in columns and rows. The data sets are produced at 3 resolutions:

* 1 by 1 degree resolution: each column contains 180 numerical values and each row contains 360 numerical values.

* 0.5 by 0.5 degree resolution: each column contains 360 numerical values and each row contains 720 numerical values.

* 0.25 by 0.25 degree resolution: each column contains 720 numerical values and each row contains 1440 numerical values.

Grid arrangement for the 1 by 1 degree data (Note arrangement is similar for other resolutions).

Grid arrangement for the 1 by 1 degree data (Note arrangement is similar for other resolutions)

	179.5 W	178.5 W	177.5 W	176.5 W	…
89.5 N	(1,1)	(1,2)	(1,3)	(1,4)	
88.5 N	(2,1)	(2,2)	(2,3)	(2,4)	
87.5 N	(3,1)	(3,2)	(3,3)	(3,4)	
86.5 N	(4,1)	(4,2)	(4,3)	(4,4)	
.					

* ARRAY(I,J)

* J = 1 IS CENTERED AT 179.5W

* J INCREASES EASTWARD BY 1 DEGREE

* I = 1 IS CENTERED AT 89.5N

* I INCREASES SOUTHWARD BY 1 DEGREE

* ARRAY_SIZE(180,360)

8.5 Related Data Sets.

- 8 km GIMMS Land Surface AVHRR data set (Tucker et al. 2003) is available directly from the GIMMS group. Please contact Dr. Tucker for this dataset.

- 1 X 1 degree, 0.5 X 0.5 degree, and 0.25 X 0.25 Normalized Difference Vegetation Index (NDVI) global data (on this DVD).

- 1 X 1 degree, 0.5 X 0.5 degree, and 0.25 X 0.25 degree IGBP SiB global land cover classification image (on this DVD).

The following datasets will be available shortly and will be provided by Ranga Myneni at Boston University.

- 0.25 X 0.25 degree biophysical parameter data sets. These data include:

- fraction of photosynthetic active radiation absorbed by the vegetation canopy (FAPAR) monthly global data.
- green leaf area index (LAI_G) global data

9. DATA MANIPULATIONS

9.1 Formulas

See 9.2.1

9.1.1 Derivation Techniques/Algorithms

See 9.2.1

9.2 Data Processing Sequence

9.2.1 Processing Steps and Data Sets

9.2.1.1 DATA SETS

These one, half and quarter degree datasets were derived from the 8 km GIMMS Land Surface AVHRR data set (Tucker et al. 2003). The data available from this dataset are:

* NDVI
* solar zenith angle
* Temperature Channel 4
* Temperature Channel 5

9.2.1.2 PROCESSING STEPS

The GIMMS NDVI data set was processed using the following steps:

1. Mapping data from NOAA 7, 9, 11 and 14 using GAPS and 16 using the KLM processing code.
2. Calibration of NOAA-7-14 data using Vermote-Kaufman (1995) and post-processing calibration using Channel 1 – Channel 2 ratio (Los 1998).
3. Satellite drift correction using Pinzon et al (2002) method.
4. Intercalibration of NDVI from all instruments using characteristics of the new generation of remote sensing instruments (MODIS, SeaWIFS, SPOT-Vegetation, etc).

Figure 1. NDVI Production Processing Steps

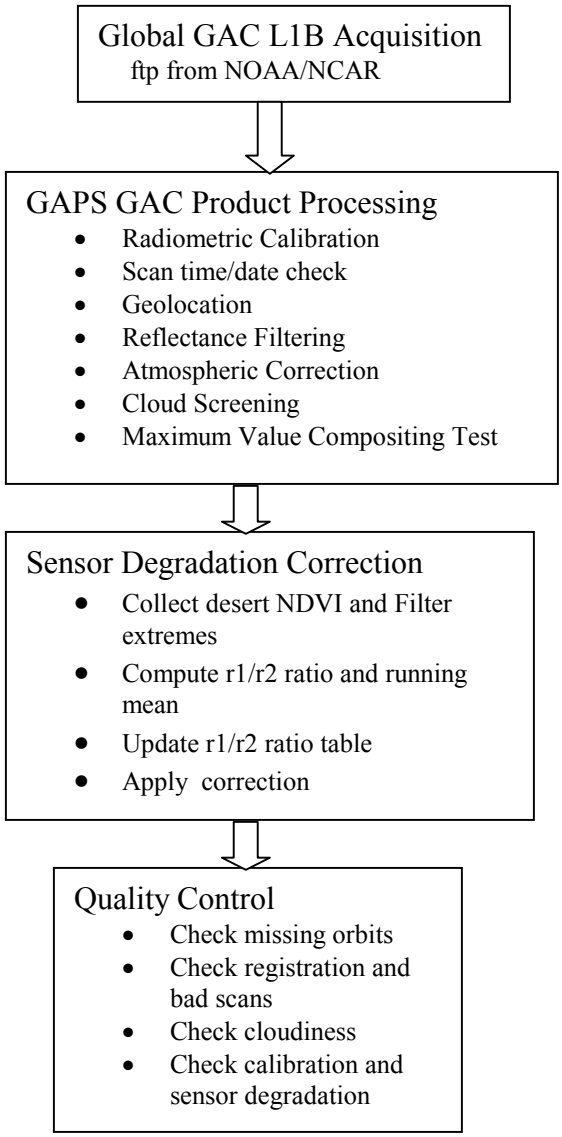

These processing steps will be discussed in correspondingly numbered steps below (this section derived from Mahoney et al (2001) and Pinzon et al (2002)).

9.2.1.2.1. **Mapping data from NOAA 7, 9, 11 and 14 using GAPS and 16 using the KLM processing code**

Compositing procedures based upon maximum NDVI value have been used effectively to minimize cloud contamination (Kaufman 1987), atmospheric effects (Holben 1986), and variations in the viewing conditions (Holben and Fraser 1984). The 8km NDVI data used to form the datasets presented here consists of maximum value composite NDVI, produced in Albers Equal area projection and binned to 8-km spatial

resolution. This dataset is characterized by bimonthly composites (days 1-15 and 16-end of the month), forward mapping, volcanic aerosol correction for 1982-1984 and 1991-1994, Vermote-Kaufman calibration, improved image navigation, and an ex post factor sensor degradation correction (see section 2) (Los 1998; Vermote and Kaufman 1995; Vermote et al. 1997).

Atmospheric Correction

Although compositing acts to minimize atmospheric effects, adverse effects due to water vapor intrusion and atmospheric aerosol contamination are evident in multi-year time-series of bimonthly and monthly composite data (Kaufman and Holben 1993). Atmospheric corrections, performed in conjunction with compositing procedures, however, without including a correction for land surface bi-directional reflectance distribution function (BRDF) may have undesirable consequences. No BRDF correction is possible with current data availability for the AVHRR sensor. Therefore, only a stratospheric atmospheric aerosol correction was performed for data affected by the El Chichon (1982-1984) and Mt. Pinatubo (1991-1994) major volcanic eruption events. The method of Vermote and El Saleous (Vermote et al. 1997) was utilized to perform the correction. Stratospheric aerosol optical thickness values utilized were based on a composite derived from that of the optical thickness data of Vermote and El Saleous (1997) and Sato (1993). The data was derived from AVHRR aerosol retrievals compared favorably with that of optical depth measurements from New Zealand; Larmie, Wyoming; American Samoa; Mauno Loa, Hawaii; and Point Barrow, Alaska (Dutton 1994) (Rosen et al. 1994) during the Mt. Pinatubo period. The data of Sato et al. (1993) derived from satellite occultation measurements for 1982-1984 and SAGE for 1991-1994 were used to extend the Vermote data set latitudinally and to fill in missing data periods.

Cloud Screening and Composite Selection Criteria

Cloud screening was performed using a simple channel 5 brightness temperature threshold of 273 degrees Kelvin for all continents except for Africa where a 283 degrees Kelvin threshold was used. Data were only pixels ± 40 degrees of nadir were selected for maximum value NDVI composites (Holben and Fraser 1984).

Image Navigation

Navigation for the NOAA-7-14 data was performed using an orbit model (Baldwin and Emory 1995) and solution of the satellite-earth view geometry (Rosborough et al. 1994) for each pixel. Starting with data from January 2000, a timing correction is applied to correct for NOAA spacecraft clock errors (Kidwell 1998). NDVI images from 1981-1999 were corrected by visual inspection and shifting of the image or by deletion of orbits associated with errors greater than 1.5 pixels (12 kilometers).

Table 1. Instrument change times for the GIMMS dataset

AVHRR instrument	Start date	End date
NOAA-7	July 1, 1981	February 8, 1985
NOAA-9	February 11, 1985	November 7, 1988
NOAA-11	November 11, 1988	September 19, 1994
NOAA-9 (descending)	September 20, 1994	January 18, 1995
NOAA-14	January 19, 1995	October 31, 2000
NOAA-16	November 1, 2000	June 30, 2002 (and continuing)

NDVI Production Processing Steps

Data from the AVHRR instruments NOAA-7, 9, 11 and 14 have been mapped using the GAPS scientific processing algorithm, which is similar to that of el Saleous (2000). We are using an earlier version of the el Saleous code that has been modified to include a forward binning procedure for NDVI, correction for volcanic aerosols, and improved robustness for rejection of data with corrupt scan lines.

Data from the AVHRR instrument NOAA-16 have the same processing steps as were outlined above with the following exceptions. The embedded datastream that is available for the KLM level 1b data format allow for the removal of the orbital model from the processing code. Fifty one geolocation points are used for every scan line to produce navigational data using a lagrangian interpolation method. In addition, time correction and roll, pitch and yaw information are available for every scan line for better navigation of the data. NOAA-16 data is not calibrated with the Vermote and Kaufman (1995) or the Los (1998) methods due to the difference in the reflectances resulting from the bilinear gains present in the data (Kidwell 2000). Preflight calibration coefficients are applied to the data before the post-processing steps are applied (steps 3 and 4 above).

9.2.1.2.2**. Calibration of NOAA-7-14 data using Vermote-Kaufman (1995) and post-processing calibration using Channel 1 – Channel 2 ratio (Los 1998).**

The AVHRR band 1 and 2 data are corrected for sensor degradation using the technique documented in Vermote and Kaufman (1995). The Vermote and Kaufman calibration reduces the relative error in the AVHRR gain as a result of sensor degradation to about 5 %. We further reduce the sensor degradation error in the gain with the technique described below, and in Los (1993, 1998).

The apparent rate of sensor gain degradation is given by:

r'_1 = rho1_s / rho1_d

where

r'_1 = apparent sensor gain degradation in band 1[1]
rho1_d = band 1 reflectance of desert sites
rho1_s = reference band 1 long-term average reflectance

We don't know the actual value of reflectance for our reflectance - invariant sites, so we assumed that the band 1 reflectance of a site is the 18-year mean value of the AVHRR band 1 reflectance for that site.

We could in a similar manner compute the degradation in the band 2 gain by

r'_2 = rho2_s / rho2_d

Instead, we employed an alternate method that expresses the degradation in the band 2 gain, r'_2, relative to the degradation in band 1 and the Simple Ratio, band 2/band 1. The advantage in using the SR to estimate the combined sensor degradation in band 1 and 2 is that residual calibration errors in the NDVI are about 1/3 smaller than when the NDVI is calculated from the calibrated component bands. This gain in accuracy can be derived from an analysis of the propagation of band 1 and 2 errors in the NDVI.

Let r'_1/2 denote the degradation in band 2 gain relative to that in band 1. That is,

r'_1/2 = r'_1 /r'_2

r'_1/2 can be expressed in terms of the simple ratio and its long-term mean, i.e.,

r'_1/2 =(rho1_s/rho1_d) (rho2_d/rho2_s) = (SR _s) / (SR _d)

where

SR _s is the variation in simple ratio over the reference sites and
SR _d is the long-term average of Pathfinder simple ratio over the reference sites

Thus we may calculate the degradation in band 2 from r'_1 and measurements of simple ratio and its long-term average.

r'_2 = r'_1 (SR _d)/(SR _s)

The calibration method and derivation of the equations is published in Los 1998. The apparent calibration coefficients for the band 1 and 2 gains were calculated for every 15-day composite. The smoothed 10-day calibration coefficients were applied to the individual bands using the inversions of the above equations.

---

[1] We refer to it as "apparent" sensor gain degradation because its value is estimated assuming that the "true" reflectance is given by the long-term average of GIMMS band 1 reflectance.

After the additional calibration corrections, the relative RMS error as a result of sensor degradation and intercalibration differences in the band 1 and 2 gains is estimated at about 1 %. The absolute calibration error is unknown, but the average calibration standard is similar to Rao and Chen (1994) and Holben et al (1990) who related their calibration standard to aircraft measurements. Vermote and Kaufman (1995) use a different calibration standard that is based on the radiative properties of the atmosphere. Because of this different calibration standard, the Vermote and Kaufman calibrated NDVI values are consistently higher than NDVIs from the other calibration methods (Vermote and Kaufman 1995).

9.2.1.2.3**. Satellite drift correction using Pinzon et al (2002) method.**

The GIMMS group uses Empirical Mode Decomposition to identify and remove parts of the NDVI signal that are most related to the satellite drift (Pinzon et al. 2003). The Empirical Mode Decomposition (EMD) was introduced by Nordon Huang in 1998 as an alternative to standard decomposition techniques for representation of nonlinear and nonstationary data that show clear physical scales or frequency content. Unlike Fourier decomposition (Trefethen and Bau 1997; Wilks 1995), the EMD a basis for the signal from the data itself. The EMD is empirical, intuitive, direct, *a posteriori*, and adaptive, with the decomposition functions based on and derived from the data (Huang et al. 1999; Huang et al. 1998). Pinzon et al. (2001) showed that EMD was applicable to NDVI time series from the AVHRR sensor to isolate orbital drift effects from the NDVI signal.

Orbital drift results in later equitorial crossing times for the NOAA satellites and results in changes of illumination that affect the NDVI. In this dataset, we identify the trends in the NDVI that associated with changes in sun-target-sensor geometry due to satellite drift. Figure 3 shows the effects of satellite drift on the Solar Zenith Angle at three latitude bands, 75-35N, 35N-35S and 35S-55S. An increasing trend is observed in each satellite due to its delay in the equatorial crossing time. This trend, overimposed on each plot, is more pronounced at lower latitude, whereas seasonal variations dominate at higher latitudes. Note that equatorial latitudes have an extra oscillation due to solar nadir moving past the target latitude, causing and increase in SZA at six month intervals rather than at yearly intervals (Privette et al. 1995).

The EMD is used to extract NDVI trends that may be caused by the satellite orbital drift, reducing the interference of other components in the NDVI signal. The EMD is used to isolate the components of the NDVI signal that are related to SZA trends and remove them from the corrected NDVI (see Figures 3 and 4). The technique removes NDVI trends that are more than 80% correlated to the SZA trends shown in Figure 3. Areas with trends that have a lower correlation are not corrected. Figure 4 shows both cases: trend removal from NDVI signal due to high correlation with the satellite drift, and trends that have not been altered because of low correlation to satellite drift.

Figure 3. Solar Zenith Angles and trends derived from the NOAA-AVHRR sensor, averaged by latitude bands 75N-35N, 35N-5S, 35S-55S

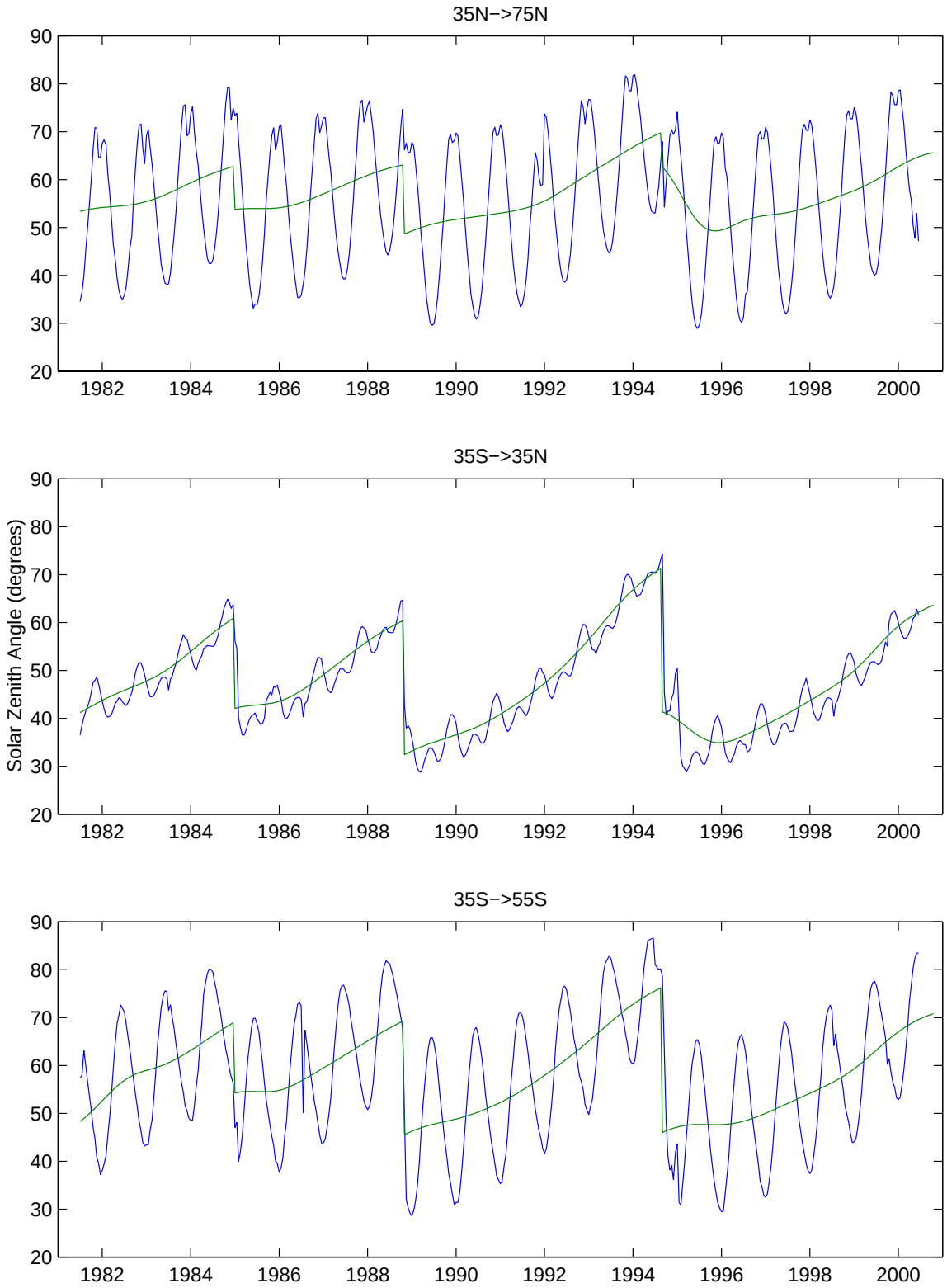

Figure 4. EMD decomposition and removal of SZA-correlated trends. A. Before satellite drift correction (series at top), trend removed (middle) and resulting series (bottom). B. Example of a pixel that is not corrected due to lack of correlation with the SZA trends.

A. B.

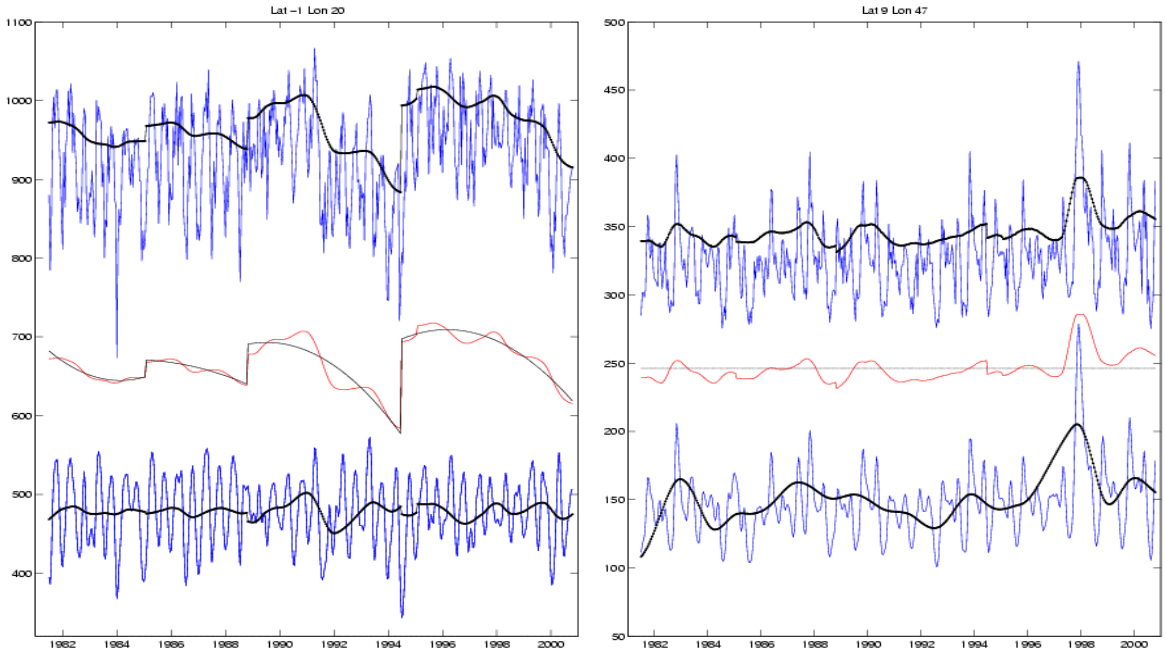

Figure 5. Regions where satellite drift has an important contribution to the signal.

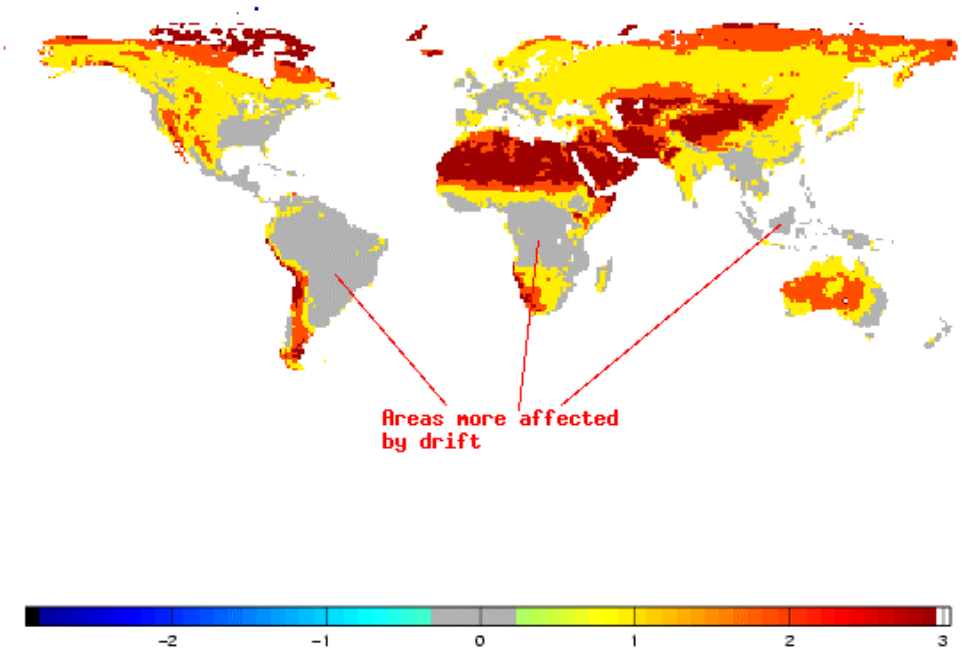

Figure 5 shows areas where the correction is the strongest, notably 1) the tropics are most affected by satellite drift due to the SZA trend magnitudes, and 2) the high northern latitude and regions with low vegetation biomes are less contaminated since the SZA component represents a small part of the NDVI signal (see Figure 3). The correction is performed by-pixel. After the satellite drift correction, a kriging interpolation removes noise and attenuates the effect of cloudy and missing pixels. The 8 km data is then averaged into 1 degree, 0.5 and 0.25 degree datasets for distribution.

9.2.1.2.4 **Intercalibration of NDVI from all instruments using narrow-band instruments such as MODIS and SPOT-Vegetation.**

In order to include the data from NOAA-16, an intercalibration of the single-gain satellites NOAA-7-14 (historical data) and the dual-gain NOAA-16 with data from SPOT-Vegetation global data at 1 km (Achard et al. 1992). SPOT data was averaged from 1 km to 8 km globally and then decomposed using the EMD method. The interannual trend from three years of data, 20 months overlapping with NOAA-14 and the rest with NOAA-16, was extracted. This trend was determined to be invariant through time over the period examined. A similar trend was extracted from the same period of NOAA-14. A non-linear regression was performed to establish coefficients that transform the historical data into the same range as that of the current and upcoming suite of visible and NIR sensors, such as MODIS, SPOT-Vegetation and others. A similar regression was performed for the NOAA-16 data. Once the trends from the historical and NOAA-16 data were transformed into the common range, the data was reconstructed and a consistent time series was established.

9.2.1.2.5. **Correction of missing data pixels**

Missing (cloudy, bad scan lines, etc) data was corrected with an interpolation from surrounding pixels using a Kriging methodology (ie every pixel will be weighted depending on its distance to and correlation with the pixel to be interpolated). The eight surrounding pixels from the current composite and the nine pixels from two previous and two subsequent composites were averaged using a weighting function to replace the missing data point. The data is then flagged with a 3 for interpolated in the QC file. If there is not sufficient data at the point to interpolate, then the data point is replaced with the seasonal component and flagged with a 5. If there is insufficient data to create a seasonal average, then the pixel will have no NDVI and will be flagged with a 7 in the QC file and a 253 in the NDVI.

9.3 Calculations

None other than the routine/normal formulas and processing sequence described in 9.1 and 9.2 above.

9.3.1 Special Corrections/Adjustments
None other than those described in 9.1 and 9.2 above.

9.4 Graphs and Plots
See text above for Graphs and Plots of the data.

10 ERRORS

10.1 Sources of Error.

Some sources of error in the NDVI data set are not accounted for with the GIMMS corrections. These errors are caused by:

- soil background reflectance; this affects low NDVI values, but does not affect high NDVI values. Thus similar low NDVI values may indicate different amounts of vegetation. However, the EMD noise removal diminishes it.

- bias as a result of compositing; this bias is smaller in the current data set than previous versions because 15-day composites were used instead of monthly composites

10.2 Quality Assessment.

10.2.1 Data Validation by Source.

Earlier versions of the GIMMS-NDVI data have been used in various models and seem to capture general patterns of vegetation well. Tests on sites showed reasonable agreement of interannnual variation in GIMMS NDVI and other measures of vegetation (rainfall variations, variations in tree-ring density (D'Arrigo et al. 2000; Davenport and Nicholson 1993; Malmstrom et al. 1997)). These tests show that the variation in GIMMS NDVI is realistic on specific sites. Comparison between climate signals and GIMMS NDVI show realistic patterns in many semi-arid regions and temperate regions. Errors in the data are thought to be most significant in areas with snow cover for a large part of the year. Comparison of the GIMMS 8km dataset with other datasets (GVI, Pathfinder AVHRR Land and with the previous GIMMS dataset) can be found in Brown et al (2003). The development of GIMMS-NDVI data is an ongoing project, further evaluation of the data is anticipated.

10.2.2 Confidence Level/Accuracy Judgment.

The GIMMS-NDVI data set is believed to give large improvements over the Pathfinder NDVI data set, especially for areas with persistent cloud cover and for needle bearing evergreen vegetation during winter. GIMMS-NDVI has reduced the effects of orbital drift, that are especially large near the end of the time of operation a satellite. Corrections for atmospheric aerosols are likely to be too small from about one to three months after an eruption (May-Jul 1982 for El Chichon and Jul-Sep 1991 for Mt Pinatubo), where the aerosols have not mixed evenly into the atmosphere.

10.2.4 Additional Quality Assessment Applied.

NDVI data are increasingly being used to assess interannual variations in the biosphere; we would like to distinguish between the following types of temporal analysis (see also Gutman 1996)

- seasonal analysis: NDVI data should have more than sufficient accuracy to assess seasonality of vegetation with great confidence. The one exception may be the small seasonal cycles observed in the Sahara, this seasonality is most likely caused by variations in atmospheric water vapor, not by variations in vegetation.

- interannual analysis: NDVI data have been used to look at year-to-year variations in desert margins (Tucker et al 1991) and to variations associated with climate oscillations (Myneni et al 1995, Los et al 2001). The interannual signal in semi-arid regions and temperate regions is in general larger than the residual errors in the data.

- trend analysis: This is in general the smallest interannual signal in the data; errors in the NDVI data are often as large or larger than the magnitude of trends, at this stage the magnitude of trends in NDVI data is uncertain within an order of magnitude.

11 NOTES

11.1 Known Problems With The Data.

The decline in NDVI in mid-1991 was due to the Pinatubo eruption and subsequent cooling and may not be related to actual declines in vegetation. Trends in tropical regions are affected by this decline and should therefore be treated with caution.

11.2 Usage Guidance.

GIMMS NDVI presents generalized patterns which may result in poor representations of a specific locale, quantitative conclusions should be drawn with caution. Nevertheless,

NDVI should provide a large improvement over previously used land cover schemes (e.g. Dorman and Sellers 1989) and NDVI data sets, because the data are collected by one series of instruments, and they give a more realistic representation of the spatial and temporal variability of vegetation patterns over the globe. Users of the data are strongly encouraged to validate their results on independent data.

11.3 Other Relevant Information.

Not available at this revision.

12 REFERENCES.

12.1 Satellite/Instrument/Data Processing Documentation and Journal Articles

References in Text:

Achard, F., J.-P. Malingreau, T. Phulpin, G. Saint, B. Saugier, B. Seguin and D. Vidal-Madjar (1992). A Mission for Global Monitoring of the Continental Biosphere: The "Vegetation" Instrument on Board "Spot 4". Toulouse, France, LERTS pp.

Baldwin, D. and W. J. Emory (1995). "Spacecraft Altitude Variations in NOAA-11 Infrared from AVHRR Imagery." International Journal of Remote Sensing **16**: 531-548.

Brown, M. E., J. E. Pinzon and C. J. Tucker (2003). "Quantitative Comparison of Four AVHRR Global Data Sets for Land Applications." Remote Sensing of Environment **under review**.

D'Arrigo, R. D., C. M. Malmstrom, G. C. Jacoby, S. O. Los and D. E. Bunker (2000). "Correlation between Maximum Latewood Density of Annual Tree Rings and NDVI Based Estimates of Forest Productivity." International Journal of Remote Sensing **21**(11): 2329-2336.

Davenport, M. L. and S. E. Nicholson (1993). "On the Relation between Rainfall and the Normalized Difference Vegetation Index for Diverse Vegetation Types in East Africa." International Journal of Remote Sensing **14**(12): 2369-2389.

Dutton, E. (1994). Aerosol Optical Depth Measurements from Four NOAA/Cmdl Monitoring Sites. Oak Ridge, Tennessee, Carbon Dioxide Information Analysis Center, Oak Ridge National Laboratory**:** 484-494 pp.

el Saleous, N. Z., E. F. Vermote, C. O. Justice, J. R. G. Townshend, C. J. Tucker and S. N. Goward (2000). "Improvements in the Global Biospheric Record from the Advance Very High Resolution Radiometer (AVHRR)." International Journal of Remote Sensing **21**(6&7): 1251-1277.

Emery, W. J., J. Brown and Z. P. Nowak (1989). "AVHRR Image Navigation: Summary and Review." Photogrammetric Engineering and Remote Sensing **55**: 1175-1183.

Holben, B. (1986). "Characteristics of Maximum-Value Composite Images from Temporal AVHRR Data." International Journal of Remote Sensing **7**(11): 1417-1434.

Holben, B. N. and R. S. Fraser (1984). "Red and near Infrared Sensor Response to Off-Nadir Viewing." International Journal of Remote Sensing **5**: 160-166.

Holben, B. N., Y. J. Kaufman and J. D. Kendall (1990). "NOAA-11 AVHRR Visible and near-Ir Inflight Calibration." International Journal of Remote Sensing **11**(8): 1511-1519.

Huang, N. E., Z. Shen and S. R. Long (1999). "A New View of Nonlinear Water Waves: The Hilbert Spectrum." Annual Review of Fluid Mechanics **31**: 417-457.

Huang, N. E., Z. Shen, S. R. Long, M. C. Wu, H. H. Shih, Q. Zheng, N.-C. Yen, C. C. Tung and H. H. Liu (1998). "The Empirical Mode Decomposition and the Hilbert Spectrum for Nonlinear and Non-Stationary Time Series Analysis." Proceedings of the Royal Society of London **545**: 903-995.

Kaufman, Y. J. (1987). "The Effect of Subpixel Clouds on Remote Sensing." International Journal of Remote Sensing **8**: 839-957.

Kaufman, Y. J. and B. N. Holben (1993). "Calibration of the AVHRR Visible and near-Ir Bands by Atmospheric Scattering, Ocean Glint and Desert Reflection." International Journal of Remote Sensing **14**: 21-52.

Kidwell, K. B. (1998). Polar Orbiter Data Users' Guide (Tiros-N, NOAA-6, NOAA-7, NOAA-8, NOAA-9, NOAA-10, NOAA-11, NOAA-12, NOAA-14), National Oceanic and Atmospheric Administration.http://www2.ncdc.noaa.gov/docs/podug/.

Kidwell, K. B. (2000). NOAA Klm User's Guide, National Oceanic and Atmospheric Administration. **2004**.http://www2.ncdc.noaa.gov/docs/klm/.

Los, S. O. (1998). "Estimation of the Ratio of Sensor Degradation between NOAA AVHRR Channels 1 and 2 from Monthly NDVI Composites." IEEE Transactions on Geoscience and Remote Sensing **36**(1): 206-213.

Mahoney, R., C. J. Tucker, A. Anyamba, M. Brown, D. Slayback, S. O. Los, J. Pinzon, J. Kendall, E. Pak, Z. Bronder, D. Grant, M. Parris and A. Morahan (2001). Global Remote Sensing of Vegetation from Space by the Nasa/Gsfc Gimms Group. International Workshop on Global Change, Tohoku University, Sendai Kyodo Printing Co. Ltd.

Malmstrom, C. M., M. V. Thompson, G. P. Juday, S. O. Los, J. T. Randerson and C. B. Field (1997). "Interannual Variation in Global-Scale Net Primary Production: Testing Model Estimates." Global Biogeochemical Cycles **11**(3): 367-392.

Pinzon, J., J. F. Pierce and C. J. Tucker (2001). Analysis of Remote Sensing Data Using Hilbert-Huang Transform. SCI 2001 Conference Proceedings.

Pinzon, J., M. E. Brown and C. J. Tucker (2003). "Nonparametric Satellite Drift Correction of NDVI Time Series from NOAA-AVHRR Radiometers Using the Empirical Mode Decomposition." IEEE Transactions Geoscience and Remote Sensing **submitted**.

Privette, J. L., C. Fowler, G. A. Wick, D. Baldwin and W. J. Emery (1995). "Effects of Orbital Drift on Advanced Very High Resolution Radiometer Products: Normalized Difference Vegetation Index and Sea Surface Temperature." Remote Sensing of Environment **53**: 164-171.

Rao, C. R. N. and J. Chen (1995). "Inter-Satellite Calibration Linkages for the Visible and near-Infrared Channels of the Advanced Very High Resolution Radiometer on the NOAA-7, -9, and -11 Spacecraft." International Journal of Remote Sensing **16**: 1931-1942.

Rosborough, G. W., D. Baldwin and W. J. Emory (1994). "Precise AVHRR Navigation." IEEE Transactions Geoscience and Remote Sensing **32**: 644-657.

Rosen, J. M., N. T. Kjome, R. L. McKenzie and J. B. Liley (1994). "Decay of Mount Pinatubo Aerosol at Midlatitudes in the Northern and Southern Hemispheres." Journal of Geophysical Research **99**(D12): 25733-25739.

Sato, M., M. Hansen, M. McCormic and J. Pollack (1993). "Stratospheric Aerosol Optical Depths, 1850-1990." Journal of Geophysical Research **98**(D12): 22987-22994.

Sellers, P., C. J. Tucker, G. J. Collatz, S. O. Los, C. O. Justice, D. A. Dazlich and D. A. Randall (1994). "A Global 1 Degree X 1 Degree NDVI Data Set for Climate Studies. Part 2." International Journal of Remote Sensing **15**(17): 3519-3545.

Sellers, P. J. (1985). "Canopy Reflectance, Photosynthesis, and Transpiration." International Journal of Remote Sensing **6**(8): 1335-1372.

Trefethen, L. N. and D. Bau (1997). Numerical Linear Algebra. Philadelphia, Society for Industrial and Applied Mathematics.

Tucker, C. J. (1980). "Remote Sensing of Leaf Water Content in the near Infrared." Remote Sensing of Environment **10**: 23-32.

Tucker, C. J., M. E. Brown, R. Mahoney, S. O. Los, N. El Saleous and E. Vermote (2003). "The Global Inventory Mapping and Monitoring 1981-1999 AVHRR 8-Km Dataset." International Journal of Remote Sensing **in review**.

Vermote, E. and Y. J. Kaufman (1995). "Absolute Calibration of AVHRR Visible and near-Infrared Channels Using Ocean and Cloud Views." International Journal of Remote Sensing **16**(13): 2317-2340.

Vermote, E., N. El Saleous, R. K. Kaufman and E. Dutton (1997). "Data Pre-Processing: Stratospheric Aerosol Perturbing Effect on the Remote Sensing of Vegetation: Correction Method for the Composite NDVI after the Pinatubo Eruption." Remote Sensing Reviews **15**: 7-21.

Wilks, D. S. (1995). Statistical Methods in the Atmospheric Sciences, an Introduction. San Diego, Academic Press.

12.3 Archive/DBMS Usage Documentation.

Contact the EOS Distributed Active Archive Center (DAAC) at NASA Goddard Space Flight Center (GSFC), Greenbelt Maryland (see Section 13 below). Documentation about using the archive or information about access to the on-line information system is available through the GSFC DAAC User Services Office.

13. DATA ACCESS

13.1 Contacts for Archive/Data Access Information
13.2 Archive Identification
13.3 Procedures for Obtaining Data
13.4 Archive/Status/Plans

14. OUTPUT PRODUCTS AND AVAILABILITY

15 GLOSSARY OF ACRONYMS

AVHRR	Advanced Very High Resolution Radiometer
CD-ROM	Compact Disk (optical), Read Only Memory
DAAC	Destributed Active Archive Center
DVD	Digital Video Disk
EOS	Earth Observing System
GAC	Global Area Coverage
GCM	General Circulation Model of the atmosphere
EMD	Empirical Mode Decomposition
FASIR	Fourier Adjusted, Solar and view zenith angle correction, Interpolation (of missing data during winter), and Reconstruction of NDVI over tropical forests.
FPAR/Fapar	Fraction of Photosynthetically Active Radiation absorbed by green vegetation
GIMMS	Global Inventory Monitoring and Modeling Studies at NASA GSFC
GSFC	Goddard Space Flight Center
GVI	Global Vegetation Index (produced by NOAA)
IDS	Interdisciplinary Science
IFOV	Instantaneous Field Of View
ISLSCP	International Satellite Land Surface Climotology Project
LAC	Local Area Coverage (1.1 km resolution)

LAI	Leaf Area Index
NASA	National Aeronautics and Space Administration
NDVI	Normalized Difference Vegetation Index
NOAA	National Oceanographic and Atmospheric Administration
PAL	Pathfinder AVHRR Land NDVI dataset
pixel	Picture element
SiB2	Simple Biosphere model (Sellers et al 1995a)
SR	Simple Ratio